CD81^{+} fibroblasts, a unique subpopulation with accelerated cellular senescence, exaggerate inflammation and activate neutrophils via C3/C3aR1 axis in periodontitis

Liangliang Fu [a,1], Chenghu Yin [a,1], Qin Zhao [a], Shuling Guo [a], Wenjun Shao [a], Ting Xia [a], Quan Sun [a], Liangwen Chen [a], Min Wang [a,*], Haibin Xia [a,*],

[a] State Key Laboratory of Oral & Maxillofacial Reconstruction and Regeneration, Key Laboratory of Oral Biomedicine Ministry of Education, Hubei Key Laboratory of Stomatology, School & Hospital of Stomatology, Wuhan University, Wuhan 430079, China; fuliangliang@whu.edu.cn (L.F.); yinchenghu@whu.edu.cn (C.Y.)

[1] These authors contribute equally to this work.

*****Corresponding author: Min Wang [a,*], Haibin Xia [a,*],

Post address: Department of Dental Implantology, School and Hospital of Stomatology, Wuhan University, 237 Luoyu Road, Wuhan, 430079, Hubei Province, PR China

E-mail addresses: xhaibin@whu.edu.cn (H.X.); 83wangmin@whu.edu.cn (M.W.)

Declaration of Competing Interest

The authors declare that they have no known competing financial interests or personal relationships that could have appeared to influence the work reported in this paper.

Abstract

Periodontitis, a prevalent inflammatory disease worldwide, poses a significant economic burden on society and the country. Despite numerous studies, the biological molecular mechanism underlying the development and progression of periodontitis remains unclear. Previous research has established a connection between cellular senescence and periodontitis. However, the role and mechanism of cell senescence in the progression of periodontitis have not been thoroughly investigated. This study aimed to explore the involvement of cellular senescence in the pathogenesis of periodontitis and determine the underlying mechanisms. Our findings demonstrated that senescent cells accumulated during the periodontitis progress and inhibiting cellular senescence in periodontitis via administration of metformin successfully alleviated inflammation and bone loss. Moreover, several scRNA-seq analysis suggested that gingival fibroblasts were the main cell population undergoing cellular senescence during periodontitis, which helps mitigate tissue damage and bone loss. Furthermore, we identified a high expression of CD81 in the senescent gingival fibroblast population. These cells were found to actively contribute to inflammation through their potent pro-inflammatory metabolic activity and secretion of SASP-related factors. Additionally, they recruited neutrophils via the C3/C3aR1 pathway, indirectly sustaining the inflammatory response. These results provide valuable insights into the cellular and molecular basis of periodontitis-induced tissue damage, highlighting the significance of fibroblast senescence. In conclusion, our study sheds light on the relationship between CD81 and cellular senescence, suggesting its potential as a therapeutic target for periodontitis.

Key words: Cellular senescence; Periodontal diseases, Human gingival fibroblasts; Senescence associated secretory phenotype; CD81

1. Introduction

Periodontitis is an inflammatory disease of irreversible progressive tissue damage, alveolar bone loss and destruction of tooth supporting tissues, and is caused by microbial infections that eventually lead to tooth loosening and eventual tooth loss (Wolff et al., 1994). Periodontitis affects 11.2% of the global population and more than 40% of people over the age of 30, posing a major burden on public health (Sanz et al., 2020) (Eke et al., 2020). Clinical studies have shown that the prevalence and severity of periodontitis increase with age, and moderate loss of alveolar bone and periodontal attachment is common in older adults (Huttner et al., 2009).

Cell senescence is a stress response characterized by irreversible proliferation arrest, resistance to apoptosis, and secretion of a range of inflammatory cytokines, growth factors, and proteases, known as senescence-associated secretory phenotypes (SASP) (Coppé et al., 2010a) (Rodier et al., 2009). Cellular senescence is considered necessary for tissue homeostasis as it aims to eliminate unnecessary damage and promote tissue repair through immune-mediated mechanisms, and even prevent the occurrence of tumors (Ohtani and Hara, 2013) (Campisi, 2013). However, the specific environment of the gingival sulcus leads to persistent plaque in periodontal tissue, resulting in oxidative DNA damage as collateral damage of chronic bacterial infection (Aquino-Martinez et al., 2020a). Repeated exposure to lipopolysaccharide (LPS) derived from *Porphyromonas gingivalis* (Pg), a key pathogen of periodontitis, can accelerate cell aging driven by DNA damage (Aquino-Martinez et al., 2021). Furthermore, recent evidence suggests that bacteria can also induce aging of healthy cells in an active oxygen-dependent manner by causing inflammation and excessive neutrophil activity (Lagnado et al., 2021). The aggravation or persistence of these stimulating factors can lead to abnormal accumulation of aging cells and directly affect periodontal tissue function. Therefore, chronic bacterial infections can cause cell senescence through both direct and indirect mechanisms.

Senescent cells have been found to contribute to bacteria-induced inflammation, with the activation of senescent cells' senescence-associated secretory phenotype (SASP) playing a crucial role in the release of various pro-inflammatory factors, including interleukin (IL)-1α, IL-6, and IL-8. Elevated levels of these inflammatory factors have been associated with periodontal damage and loss of alveolar bone (Aquino-Martinez et al., 2020a). However, the specific mechanism by which senescent cells contribute to the development of periodontitis remains unclear. In the

immune response to periodontitis, dendritic cells (DCs) infected by Pg activate related SASPs, such as IL-1β, IL-6, and IL-8, which ultimately accelerate the progression of periodontitis (El-Awady et al., 2022). Additionally, the aging of T lymphocytes, which are crucial for adaptive immunity, leads to a significant alteration in their immunosuppressive ability in Th17/Treg subsets. This alteration ultimately results in the loss of tooth support and alveolar bone (González-Osuna et al., 2022). However, the role and mechanism of cellular senescence in the progression of periodontitis have not been thoroughly investigated.

The breakthrough technology of single-cell RNA sequencing has made it easier to analyze gene expression at the cellular level and identify key cell subpopulations (Zhang et al., 2021). In this study, we utilized bulk-RNA seq, clinical periodontal samples, and a mice ligature-induced periodontitis model to demonstrate that cellular senescence levels increase with periodontitis progression. We also found that targeting cellular senescence with anti-aging drugs can reduce inflammation and delay alveolar bone resorption in periodontitis. Through sc-RNA seq, in vitro, and in vivo experiments, we observed significant cellular senescence in gingival fibroblasts. Additionally, we identified a unique subgroup of gingival fibroblasts with high expression of CD81, which exhibited aging characteristics such as ROS accumulation and enrichment of aging genes. We propose that this subgroup of fibroblasts can directly promote the progression of periodontitis by secreting SASP-related factors, such as IL-6, and indirectly amplify inflammation by recruiting neutrophils through the complement pathway, specifically C3.

Error! Bookmark not defined.. **Results**

2.1 Accelerated cellular senescence in periodontitis

By detecting the expression of aging markers P16 (Fig. 1A) and P21 (Fig. 1B) in human periodontitis gingival tissue, an increase in positive signals in the lamina propria of periodontitis gingival tissue was observed, indicating accelerated aging in periodontitis. To further illustrate the variation of cellular senescence during periodontitis, we established a mouse model of ligature-induced periodontitis (LIP) (Fig. 1C). We found that the level of aging in gingival tissue continued to increase throughout the development of periodontitis, and the expression level of P16 was significantly upregulated between day 3 and day 7 (Fig. 1D). Subsequently, by detecting the expression levels of P16 protein (Fig. 1E) and p16, p21, and p53 transcription (Fig. 1F) in gingival tissue at a critical time point of 7 days post-ligature, an upward trend can also be detected.

Moreover, bulk RNA-sequencing was performed on the gingival tissue, and aging-related genes were detected among the upregulated genes (Fig. 1G). GSEA enrichment analysis revealed the upregulation of the aging pathway (Fig. 1H). Additionally, after GO analysis of differential genes, upregulation of the aging pathway (arrow) (Fig. 1I) was found, along with upregulation of a series of related inflammatory pathways. These findings collectively suggest that aging at the cellular level accumulates along with periodontitis progression, providing a potential target in the treatment of periodontal disease.

2.2 Inhibition of cellular senescence alleviated periodontitis progression

Metformin, an anti-aging drug, has shown potential in inhibiting cell senescence in various disease models. In order to investigate its potential in alleviating periodontitis progression by targeting aging, we analyzed single cell RNA sequencing data of GSE242714 from gingiva tissue of periodontitis mice treated with metformin. The results indicated that metformin could reduce the aging characteristics of the overall gingiva (Neves et al., 2023) (Supplementary Fig. 1A). Additionally, we established a LIP mouse model and administered metformin daily for 14 days before and after the modeling time point. Micro-CT images revealed delayed bone loss around the periodontal area after metformin administration (Fig. 2B). The BV/TV ratio (Fig. 1Ga) and alveolar bone height (CEJ-ABC distance, Fig. 2Gb) both confirmed the protective effect of metformin in periodontitis. Histological analysis further demonstrated that metformin significantly alleviated periodontitis-induced bone resorption damage, inflammatory cell infiltration (Fig. 2C), and collagen degradation (Fig. 2D) as observed through H&E and Masson staining. Moreover, metformin administration reversed the upregulation of P16 (Fig. 2E) and P21 (Fig. 2F) expression in periodontitis models. These findings suggest that targeting the aging process could be an effective strategy for the treatment of periodontitis.

2.3 Gingival fibroblasts were the main cell type responsible for cellular senescence in periodontitis

To investigate which cell type among periodontal tissue exhibited enrichment of cell senescence in the context of periodontitis, single cell RNA sequencing analysis of human gingiva was conducted (Williams et al., 2021).The gingival cells were clustered into 15 distinct groups, each identified by specific cell markers (Supplementary Fig. 2A, B). These clusters were further classified as fibroblasts, immune cells, epithelial cells, endothelial cells, and other cell types (Fig.

3A). In periodontitis gums, there was a notable change in the cellular composition, with a higher proportion of immune cells and a decrease in other cell types (Fig. 3B). Fibroblasts were found to be the primary cell type exhibiting senescence gene set up-regulation in periodontitis, indicating the highest overall average level of senescence (Fig. 3D). GSEA enrichment analysis of differentially expressed genes in periodontitis versus healthy fibroblasts also confirmed the upregulation of the senescence pathway (Fig. 3C). Moreover, data analysis from GSE152042 showed an increase in senescence characteristics of fibroblasts with the severity of periodontitis (Fig. 3E) (Supplementary Fig. 2C, D). Immunofluorescence results further supported the presence of senescence in human and mouse gingival fibroblasts during periodontitis (Fig. 3F, G). In vitro experiments with healthy primary gingival fibroblasts (HGF) stimulated with LPS-PG at different concentrations and times demonstrated a time/dose dependent increase in the expression of senescence-associated markers, such as Positive of senescence Associated β-galactosidase (SA-β-gal) (Fig. 3H) and P16 mRNA levels (Fig. 3I). However, treatment with metformin led to a decrease in the positive rate of SA-β-gal in HGF stimulated by LPS-PG, indicating a potential role of metformin in reducing senescence (Supplementary Fig. 2E). The above results indicated that gingival fibroblasts were the main cell type characterized by senescence in the development of periodontitis lesions.

2.4 CD81+ fibroblasts were identified as the major fibroblast subpopulation undergoing senescence

To investigate the changes in subpopulations of gingival fibroblasts in periodontitis, we divided gingival fibroblasts into 7 subpopulations (Fig. 4 A). The cell proportion bar chart illustrated a significant increase in the proportion of subpopulation 1 and 3 in periodontitis (Fig. 4 B). Moreover, we performed aging-related gene set scores on these subpopulations and found that subpopulation 1 exhibited the highest average expression level, showing a significant increase in periodontitis (Fig. 4 C). Additionally, we conducted enrichment analysis on the differentially expressed genes among different subgroups of fibroblasts. Pathway analysis revealed upregulation of the pathways related to low oxygen and elevated reactive oxygen species levels in subpopulation 1 (Fig. 4 D). GO enrichment analysis further demonstrated that subpopulation 1 exhibited an upregulation of aging characteristics (Fig. 4 E), suggesting that it is the main subpopulation of fibroblasts undergoing senescence. For future research, we utilized the CD81

protein located on the membrane of the top 20 marker genes in subpopulation 1 as the marker gene for this subpopulation, which we named the CD81-positive cell group (Fig. 4 F). The density heatmap revealed that CD81 was enriched in group 1 (Fig. 4 G). The other subgroups were defined as EmFB (Extracellular matrix associated fibroblasts), P-EmB (Pre Extracellular matrix associated fibroblasts), MyFB (myofibroblast), P-MyFB (Premyofibroblast), VFB (Vascular associated fibroblasts), and ImFB (Immune associated fibroblasts) through GO analysis (Fig. 4 H). Immunofluorescence staining results demonstrated a high co-localization of CD81 and the fibroblast marker Vimentin, with their proportion increasing in periodontitis (Fig. 4 I and J). Tricolor fluorescence co-staining of CD81, Vimentin, and P16 also revealed the presence of highly co-localized cell populations in periodontitis (grey arrow) (Fig. 4 K). The expression levels of P16 and P21 increased in a concentration-dependent manner upon LPS stimulation, which correlated with the increase in CD81 expression (Fig. 4 L). Therefore, CD81+ fibroblasts were identified as a core subgroup of cell senescence.

2.5 CD81^{+} fibroblasts were terminally differentiational cell with high SASP expression and metabolism alteration

To investigate the role of CD81+ fibroblasts in periodontitis inflammation, it is important to consider the senescence-related secretory phenotype (SASP), which is a key characteristic of aging cells. Many molecules associated with SASP have strong pro-inflammatory properties. Analysis of gene expression levels related to SASP in different subgroups of fibroblasts revealed that CD81+ fibroblasts exhibit high expression levels of SASP-related genes such as IL-6, CXCL-5, CXCL-6, MMP1, and MMP3 (Fig. 5 A). Additionally, the metabolic activity of each subgroup of fibroblasts was examined, specifically focusing on lipid metabolism. It was found that pathways related to the metabolism of linoleic acid, linolenic acid, arachidonic acid, and steroid biosynthesis were significantly upregulated in CD81+ fibroblasts (Fig. 5 B). This trend of metabolic pathways was similar to the development of periodontitis (Fig. 5 C), suggesting that the activation of lipid metabolism pathways may be involved in the progression of periodontitis. Notably, arachidonic acid can be converted into prostaglandins and leukotrienes through COXs and lipoxygenases, which further contribute to the inflammatory response (Fig. 5 D). Moreover, the expression of COX1 and COX2 was significantly increased in CD81+ fibroblasts (Fig. 5 E). The differentiation trajectories of fibroblasts were analyzed using pseudotime analysis, which

revealed the subpopulations of fibroblasts (Fig. 5F and G). The CD81 positive cell population was mainly found at the end of the differentiation trajectory, indicating its limited differentiation ability. By clustering the gene expression time module and conducting functional enrichment analysis on a group of genes that gradually increased in expression during differentiation, we observed an increase in inflammatory activation and aging characteristic pathways (Fig. 5 H). Additionally, this group of genes included SASP genes (Fig. 5 I). Overall, our bioinformatics analysis demonstrated that the cellular senescence of CD81+ fibroblasts could be attributed to disturbances in lipid metabolism, resulting in differentiation arrest and higher expression of SASP factors in CD81+ fibroblast cells.

2.6 CD81+fibroblasts indirectly sustained inflammation by recruiting neutrophils via C3/C3aR1 axis

To investigate the communication between CD81+ fibroblasts and other immune cells, we examined their interaction in periodontitis. Our results showed that CD81+ cells had the highest proportion of immune cell communication, particularly with neutrophils. This suggests that CD81+ cells play a significant role in mediating immune response in periodontitis (Fig. 6 A) (Supplementary Fig. 3A, B). We observed a significant increase in the expressions of MIF, MKD, and C3 receptor pairs between CD81+ cells and immune cells (Fig. 6 B). Previous studies have demonstrated the importance of sustained neutrophil infiltration in the progression of periodontitis, and C3 has been shown to recruit neutrophils and contribute to the formation of Neutral extracellular traps (Yipp et al., 2012). By analyzing the C3 pathway alone, we found that the C3 complement receptor pair pathway was most active in CD81-positive cell-to-neutrophil communication in both healthy and periodontitis conditions (Fig. 6 C), highlighting its unique role in neutrophil recruitment. Additionally, we observed the highest expression of C3 ligand in CD81+ cells (Fig. 6 D). Furthermore, we detected the presence of C3 and MPO positive cells in human and mouse periodontitis gingiva (Fig. 6 E) (Supplementary Fig. 3C), indicating their involvement in the disease. Immunofluorescence analysis revealed a high co-localization of CD81 and C3, with an increased proportion of double positive cells (Fig. 6 F). Interestingly, CD81 and MPO positive cells were found to be closely adjacent in space (Fig. 6 G). The analysis of spatial transcriptome data from periodontitis and healthy gingival tissues revealed that CD81 and MPO-rich regions in periodontitis were located in the gingival lamina propria and exhibited a high

spatial coincidence (Fig. 6 H and I) (Supplementary Fig. 3E). These findings suggest that CD81-positive cells have the ability to attract neutrophils through C3. Interestingly, the expression levels of C3 and MPO in periodontitis could be reversed with metformin administration, as compared to the periodontitis and ddH20 group (Fig. 6 J, K). In vitro results also demonstrated that metformin could reverse the expression of CD81, C3, and P16 (Supplementary Fig. 4A). Similarly, the addition of metformin could simultaneously reduce the proportion of CD81 with P16 and CD81 with C3 double-positive gingival fibroblasts (Supplementary Fig. 4B, C). Overall, these findings propose a novel mechanism by which CD81+ fibroblasts enhance neutrophil recruitment via C3.

3. Discussion

This study suggests that cellular senescence plays a role in the progression of periodontitis, and targeting cellular aging may help alleviate the condition. The researchers discovered that senescent gingival fibroblasts are associated with periodontitis pathology. Under continuous stimulation of LPS-PG, oxidative stress caused by reactive oxygen species (ROS) accelerates cell senescence in gingival fibroblasts. These senescent cells highly express CD81. They contribute to the expansion of inflammation through proinflammatory metabolic activities and factors related to senescence-associated secretory phenotype (SASP). Additionally, they continuously recruit neutrophils through the C3 pathway, indirectly maintaining the inflammatory response. The use of metformin can slow down the progression of periodontitis by reducing gingival cell senescence (Fig. 7).

The underlying mechanism of immune homeostasis instability and the transformation of chronic gingivitis into periodontitis has not been fully elucidated. Our findings will provide valuable insights for future studies on the pathological mechanism of periodontitis development. Gingival fibroblasts, which are essential cells in gingival connective tissue, have recently gained attention as key participants (Wielento et al., 2023). Previous studies have reported heterogeneity in gingival fibroblasts in periodontal tissues, with four subsets significantly altered in periodontitis: Fib1.1 (CXCL1, CXCL2, CXCL13); Fib 1.2 (APCDD1, IGFBP2, MRPS6); Fib 1.3 (APOD, GSN, CFD); and Fib 1.4 (TIMP3, ASPN, COL11A1). Some of these clusters are directly associated with neutrophils and proinflammatory cytokines, suggesting that periodontal tissue immunity relies on strong matrix-neutrophil interactions within these tissues (Williams et al., 2021). Another study

revealed the presence of genetic markers in a unique subgroup of gingival fibroblasts called AG fibroblasts (fibroblasts activated to guide chronic inflammation). These fibroblasts may have functional capabilities as oral immune surveillance agents and play a role in coordinating the initiation of gingival inflammation (Kondo et al., 2023). Caetano et al. (2021) conducted a study where they mapped stromal cells from healthy and periodontitis individuals. They identified a subset of fibroblasts that expressed ARGE pro-inflammatory genes at high levels. In a more recent study, the team used multiomics techniques and fluorescence in situ hybridization to demonstrate the presence of a spatially restricted population of pathogenic fibroblasts in the gingival lamina propria. These fibroblasts expressed CXCL8 and CXCL10 and were responsible for recruiting neutrophils and lymphocytes in the periodontal pocket area. Additionally, they exhibited angiogenic properties (Caetano et al., 2023). The increasing amount of data supports the role of gingival fibroblast heterogeneity in the pathological mechanism of periodontitis, particularly in immune regulation. However, previous studies have mainly focused on immune disorders resulting from communication between fibroblasts and immune cells, neglecting the dynamic changes of fibroblasts themselves in periodontitis pathology. In this study, we present a unique subset of fibroblasts with significantly altered gene signatures due to cell senescence, suggesting that cell senescence plays a crucial role in the heterogeneity of gingival fibroblasts.

It has been recognized that low concentrations of reactive oxygen species (ROS) produced during chronic inflammation can indirectly cause periodontal tissue destruction (Chapple and Matthews, 2007). Recent studies have also found that repeated exposure to lipopolysaccharide (LPS), a component of gram-negative bacterial membranes, leads to DNA damage in various cell types, including gingival and alveolar bone cells (Aquino-Martinez et al., 2020b). Cells that survive persistent DNA damage acquire a senescent phenotype, which in turn triggers the recruitment of immune cells through dysregulation of proinflammatory cytokines. Senescent cells often overexpress interleukin-6 (IL6), IL1 α, IL1 β, and IL8, collectively referred to as senescence-associated secretory phenotype (SASP) (Coppé et al., 2010b). Our findings indicate that gingival fibroblast senescence directly promotes the development of chronic periodontitis by secreting SASP-related factors, which may explain the formation of pro-inflammatory fibroblasts and their significant impact on immune regulation. Accumulating evidence suggests that drugs can regulate the activity of SASP, as demonstrated by An et al. who showed that short-term treatment

with rapamycin can reduce gingival and alveolar bone inflammation and promote the regeneration of alveolar bone in elderly mice (An et al., 2020). Additionally, Kuang et al. reported that metformin inhibits the destructive effect of H_2O_2 on human PDLSC, leading to a reduction in oxidative stress-induced aging (Kuang et al., 2020). Through oral administration of metformin, we have demonstrated its potential in alleviating the progression of periodontitis by delaying the aging of gingival fibroblasts. However, further experiments are required to determine the decisive role of fibroblast aging in the overall aging cell population.

CD81, a member of the tetraspanin family of proteins, could serve as a cell surface marker (Karam et al., 2020) and a signaling pathway receptor (Oguri et al., 2020). CD81 is a major regulator of virus entry into cells and plays an important role in other pathogenic human viruses (New et al., 2021). Research on the role of CD81 has shown that it could form a complex with αV/β1 and αV/β5 integrins to activate the FAK signaling pathway (Oguri et al., 2020), induce the interferon signaling pathway for immune response regulation (Hanagata and Li, 2011), and mediate NF-kB signaling pathway to induce IL-6 expression (Ding et al., 2019). Clinical studies have indicated a correlation between the level of CD81 in saliva and the severity of periodontitis disease (Tobón-Arroyave et al., 2019), as well as its association with the regulation of aging and inflammation (Jin et al., 2018). In our study, we observed that gingival fibroblasts with high CD81 expression exhibited a high enrichment of the NF-kB signaling pathway, leading to significant upregulation of IL-6 expression. The NF-kB pathway is recognized as a switch for cellular senescence, and NF-kB activation can drive cell senescence-related secretory phenotypes (Wang et al., 2022). Therefore, CD81 is likely to play a crucial role in regulating gingival fibroblast cell senescence. However, further investigation is needed to elucidate the specific molecular mechanism.

Finally, a link has been established between complement C3 from senescent fibroblasts and neutrophil infiltration in periodontitis. C3 has a strong recruitment ability for neutrophils and is crucial for the formation of neutrophil extracellular traps (NETs) (Yipp et al., 2012). Persistent neutrophil infiltration and hyperresponsiveness, including the formation of NETs, play significant roles in the development of periodontitis (Uriarte and Hajishengallis, 2023). Genetic analysis and preclinical studies have confirmed C3 as a potential pharmacological target for periodontitis treatment (Alayash et al., 2023; Hajishengallis et al., 2021). gingival fibroblasts stimulated with

IFN-γ (GF(IFN-γ)) up-regulated the expression of chemokines (CXCL9, -10, -11, CCL8), molecules involved in antigen presentation, complement component 3 (C3), and other immune response-related molecules (Ha et al., 2022). Our experimental results have demonstrated that CD81+ gingival fibroblasts are an important source of C3. Understanding the source and mechanism of C3 complement in periodontitis is of great significance for comprehending the pathological development of the disease and can provide a new perspective for designing drug schemes.

Our study focused on identifying a specific group of gingival fibroblasts that express high levels of CD81 during the development of periodontitis. Our findings suggest that these CD81+ gingival fibroblasts exhibit characteristics of aging and possess strong pro-inflammatory abilities. Furthermore, we have established a connection between CD81+ gingival fibroblasts and the recruitment and hyperactivation of neutrophils through complement C3. However, further investigations are required to explore the association between CD81 and cellular senescence, as well as its potential as a therapeutic target. In conclusion, our research provides valuable insights and treatment strategies for understanding the progression of periodontitis.

4. Materials and methods

4.1 Human samples

All individuals provided written informed consent and this study was approved by the Ethics Committee of School & Hospital China Hospital of Stomatology Wuhan University [WDKQ2024]. A total of 16 participants were recruited (healthy group: n = 8, 24 ± 3 years of age; n = 8, 52 ± 8 years of age). All included patient basic information were listed in Supplementary Table 1. Healthy control group included crown lengthening procedures, and inclusion criteria are as follows: The standard of healthy gum as follow, 1) age 18-40 years old; 2) good general health, no systemic diseases, able to tolerate periodontal surgery; 3) no erythema, edema, bleeding and other symptoms in gingival tissue; 4) no use of nicotine-related products in recent 6 months. Periodontitis group included patients who went through pocket reduction surgeries. Inclusion criteria for patients with chronic periodontitis were as follows: 1) age 18-35 years; 2) good general health, no systemic disease, and tolerance to periodontal surgery; 3) mild gingival tissue redness, bleeding on probing, or clinical attachment loss (CAL) ≥ 4 mm or probing depth (PD) ≥ 5 mm in non-acute inflammatory periods; 4) no use of nicotine-related products in the last 6 months.

4.2 Primary gingival fibroblast cell culture isolation and culturing

Gingiva tissues were transported from the clinic to the laboratory in phosphate-buffered saline (PBS) solution, washed with 70% ethanol and rinsed in PBS several times to remove the ethanol. And then, the tissues were minced into small fragments of approximately 1–3 mm. The tissue pieces were placed in cell culture dishes and digested with 1 mg/ml type I collagenase (Sigma, St. Louis, MO, USA) B. Sun, S. Ying, Q. Ma et al. + MODEL at 37℃ for 1 h, and incubated for 5–7 days at 37℃ and 5% CO2 in DMEM high-glucose medium (DMEM, YC-2067, China) supplemented with 20% fetal bovine serum (FBS, PAN-SERATECH, South America). The Primary gingival fibroblast cells that grew out of the explants were cultured and maintained. Gingival fibroblasts at passages four to eight were used in the following experiments.

4.3 Cells treatment with metformin

HGFs (150,000 cells per ml using Hemacytometer) were seeded in 3 ml plates and incubated in complete medium at 37 °C overnight. Except for the control sample, cells were treated with various concentrations of Met (2 mM) for 24 h. Cells were also stimulated with Pg LPS (InvivoGen, San Diego, CA) according to a previous study for another 24 h. Subsequently, HGFs cells were harvested for subsequent RNA and protein extractions.

4.4 Staining for Senescence-Associated Galactosidase (SA-β-gal)

SA-β-gal staining was performed using the Senescent β-Galactosidase Staining Kit (C0602; Beyotime Biotechnology, China) according to the manufacturer's instructions, and incubated overnight at 37°C in a CO_2-free temperature chamber for 12 hours. Positive blue-stained cells were counted under an ordinary light microscope (DP72 microscope, Olympus, Japan). Results were expressed as the percentage of positive cells. Nine randomized regions of interest were captured from each group and positive cells were counted by Image J v2.0 (NIH, Bethesda, MD, USA).

4.5 Mouse model of ligature-induced periodontitis

C57BL/6 mice (8 weeks, male) were purchased and bred. The animal tests in this study adhere to the guidelines established by the Animal Research Ethics Committee at the School & Hospital of Stomatology, Wuhan University, China (No. S07922040A) and followed the ARRIVE guidelines 2.0. Animals were housed in a specific pathogen free environment with controlled temperature/humidity with 12 h light/dark cycle. In brief, after anesthetics, the

ligature-induced periodontitis group were ligated with a 5-0 silk (SA82G, ETHICON, China) between the maxillary left first and second molars and knots were tied on both ends to secure the ligature. The distance between the two knots is about 2.5mm. The ligatures were examined daily to ensure that they remained in place during the experimental period. Periodontal inflammation and bone loss in this model is initiated by massive local accumulation of bacteria on the ligature-treated molars. For group allocation, except for the Ligature Met (LIP + Met) and the Control MET (CON+ Met)) groups treated with 200 mg/kg metformin, the distilled water was used as the control in the Control (CON + ddH_2O) and Ligature groups (LIP + ddH_2O). All the treatments were given by intragastric administration once a day for 14 days. On the fifteenth day after intragastric administration, the Ligature and Ligature Met groups were ligated with a 5-0 silk between the maxillary left first and second molars and knots were tied on both ends to secure the ligature. A second set of controls included mice that were not treated with ligatures on either side. Four groups of mice were placed in the LIP model or control group for 14 days, ligations were placed at the beginning of the experimental time frame formation, injections were given daily during the 14 days, at the end of the time frame mice were euthanized and their maxilla and gums were collected.

4.6 Micro-tomographic (micro-CT) scanning and analysis

Micro-CT scanning was performed using Bruker Micro-CT SkyScan1276 (Konitich, Germany). The region of interest (ROI) was established in a three-dimensional (3-D) scope: vertically, starting from 0.2 mm apical to the cemental enamel junction (CEJ) of the 2nd M, extending towards the root apical to get a span of 0.5 mm; mesiodistally, ranging from the most mesial aspect of the CEJ of the first molar(1st M) to the root furcation of the third molar (3rd M); buccolingually and lingually, ranging around the root furcation of the 2nd M within a span of 1.5 mm. The ratio of bone volume to total volume (BV/TV) was calculated based on this ROI. The distances between the CEJ to the alveolar bone crest (CEJABC) were measured at the 1st M and 2nd M separately. The 3-D reconstruction, calculation and measurements were conducted using the Object Research Systems (ORS) Dragonfly software (version 2022.1, Montreal, Canada). All measurements were repeated for three times with N = 6.

4.7 Protein extraction and western blot

Protein extracted from human samples or Primary gingival fibroblasts and were dissolved in 80 μL of RIPA buffer to extract total protein, supplemented with protease and 1% phosphatase inhibitors. All samples were quantified and normalized using a protein assay kit known as bicinchoninic acid (Thermo Fisher Scientific, Waltham, MA, United States). Following a 10-minute heat treatment at 95 ℃, the samples underwent sodium dodecyl sulfate-polyacrylamide gel electrophoresis for separation and were then transferred to a polyvinylidene fluoride membrane (Millipore). The membrane was blocked using the primary antibody-blocking solution and then incubated overnight at 4 ℃ with primary antibodies against P16, P21, CD81, β-actin, C3,and GAPDH (ABclonal, China). Subsequently, the membrane was treated with horseradish peroxidase (HRP) conjugated secondary antibodies at 37 ℃ for 1 h. Visualization of signals were conducted using a Ultrasensitive ECL Detection Kit (Thermo Fisher Scientific, Waltham, MA, United States) with the ChemiDoc MP Imaging Systems (Bio-Rad, USA). Protein levels were normalized to β-actin using Image J analysis software.

4.8 RNA extraction and RT-qPCR

To extract total RNA, the Trizol reagent and standard collection procedure were utilized [24]. Total RNA concentration was measured using a Nanodrop2000 instrument (Thermo Fisher Scientific, Waltham, MA, United States). According to the guidelines provided by the manufacturer, the total RNA was subjected to reverse transcription into cDNA using the HiScript II Q RT SuperMix (Vazyme). The amplification reaction was performed using ChamQ SYBR qPCR Master Mix (Vazyme) in the QuantStudio 6 Flex System (Thermo Fisher Scientific, Waltham, MA, United States). The primers for the experiment were bought from Sangon Biotech Co., Ltd. The results were analyzed using the $2^{-\Delta\Delta Ct}$ method, with normalization to β-actin or Gapdh and calibration to the control group. The forward and reverse primer sequences of the target genes used in the experiment can be found in Table S2.

4.9 Histological analysis

The maxilla with gingival tissues were kept in 4% paraformaldehyde for 24 h, followed by 4 weeks of decalcification with 15% EDTA at pH 7.4. The decalcifying solution underwent replacement every 2 days. Tissues were then sectioned, fixed in paraffin, and dehydrated. According to the manufacturer's instructions, immunohistochemical, Masson, hematoxylin and eosin (H&E) staining were performed (MXB biotechnologies, Fuzhou, China). The primary

antibodies used for immunohistochemistry were P16 (1:1000; Cat: 10883-1-Ap, Proteintech, China), P21 (1:200, Cat: 10355-1-AP, Proteintech, China) and C3 (1:200, Cat: 21337-1-AP, Proteintech, China) and MPO (1:200, Cat: Ab208670, Abcam). Immunofluorescence (IF) staining was performed with the antibodies of CD81 (1:1000, Cat: 10883-1-AP, Proteintech, China), Vimentin (1:200, Cat: A19607, ABclonal, China), P16, C3 and MPO as previously described. To perform immunohistochemical staining (IHC), we utilized 3,3-diaminobenzidine tetrahydrochloride (Zhongshan Biotechnology, Ltd, China) to visualize color development. For double IF staining, anti-mouse, and rabbit secondary antibodies had Cy3 red and 488 nm green fluorescent markers (ABclonal, China). For triple IF staining, the nucleus of cells in tissues was stained using DAPI (Zhongshan Biotechnology, Ltd, China). The stained sections were examined and captured using an Olympus DP72 microscope (Olympus Corporation, Japanese).

4.10 Bulk RNA sequencing

For bulk RNA sequencing, RNA was obtained as described in qRT-PCR methods. Following this, total RNA was sent to the Oxford Genomics Centre (Oxford, United Kingdom) for quality control, library preparation and sequencing using Illumina platform, The fastq reads where aligned to the mouse genome (GRCm38) using an RNAseq specific aligner. Raw data quality was filtered using Trimmomatic (version 0.36), filtered Reads were aligned to the reference genome using HISAT2[1] (version 2.2.1), and aligned Reads were quantified using StringTie [2]. For those with biological duplication, we used DESeq2 [8] (version: 1.34.0) to screen differentially expressed gene sets between two biological conditions; for those without biological duplication, we used edgeR [9] (version: 3.36.0, dispersion parameter: 0.01) for analysis. We first used Fold Change ≥ 2 and FDR < 0.05 to screen for differential genes.

4.11 Single-cell RNA sequencing analysis

Single-cell RNA transcriptome including GSE164241, GSE152042 and GSE242714 were obtained from the GEO dataset. GSE164241 contained 70407 cells from 8 healthy samples and 13 periodontitis samples. GSE152042 contained 12379 cells from 2 healthy samples ,1 periodontitis sample (mild) and 1 periodontitis sample (severe). GSE242714 contained 6473 cells from the control mice and LIP mice samples, which were put on either water or Metformin samples (n = 5 group). As for scRNA-seq, the “Seurat4.4.0” package was applied to integrate different samples with CCA (cross-dataset normalization) method, GSE164241 cell profiles were filtered scriteria of

Feature_RNA> 200 & nFeature_RNA <5000 & MT_percent <10 & nCount_RNA<25000 & nCount_RNA > 1000, then GSE152042 cell profiles were filtered scriteria of Feature_RNA> 500 & nFeature_RNA <6000 & MT_percent <20, and GSE242714 cell profiles were filtered Feature_RNA> 300 & nFeature_RNA <5000 & MT_percent <15 & nCount_RNA<25000 & nCount_RNA > 500 , then those data were further normalized using the "LogNormalize"method, and the unique gene markers in each group were identified with the "FindMarkers"function.“UMAP” was used to display the cell distribution. The function "Addmodulescore" was used to reflect differences in biological processes in different cell populations.

4.12 Fibroblast cell re-clustering analysis

Fibroblast clusters were identified as being ‘collagen producing’. These two clusters were reanalysed separately from the integrated dataset. Datasets were then re-normalised by calling the ‘NormalizeData’ function to account for the reduction in cell numbers subsequent to subsetting the data. According to the author instructions, the top 2000 most variable features across the dataset were then identified using the ‘FindVariableFeatures’. These variable features were subsequently used to inform clustering by passing them into the ‘RunPCA’ command. Using ‘Elbowplot’ we identified that the first eight principle components should be used for downstream clustering when invoking the ‘FindNeighbors’ and ‘RunUMAP’， as detailed above.

4.13 Gene function enrichment analysis

Gene ontology (GO) analysis was performed using Enrich on the top 200 differentially expressed genes (adjusted p-value < 0.05 by Wilcoxon Rank Sum test). GO terms shown are enriched at FDR < 0.05. The enrichment analysis between different fibroblast subsets in scRNAseq was performed by Metascape and further drawn by the ggplot2 package in R. Four methods including ssGSEA, AUCell, UCell, and singscore were used for enrichment analysis between different clusters. Images were further drawn by "irGSEA". Gene set enrichment analysis (GSEA) was applied to validate the result on RNA-seq with default settings (1000 permutations for gene sets, Signal2Noise metric for ranking genes).

4.14 “aging” and “Senescence-associated secretory phenotypes” gene set

The aging gene set, which was used to reflect the degree of cellular senescence, has been validated across species in a variety of cell lines and multiple sequencing data including

scRNA-seq, bulk RNA-seq, etc. It has better validation efficiency than previously known gene sets associated with cell senescence(Saul et al., 2022). SASP(Senescence-associated secretory phenotypes) includes several soluble and insoluble factor families，These factors can affect surrounding cells by activating various cell surface receptors and corresponding signal transduction pathways that may lead to a variety of pathologies. SASP factors can be divided globally into the following main categories: soluble signal transduction factors (interleukins, chemokines and growth factors), secreted proteases and secreted insoluble protein/extracellular matrix (ECM) components (Coppé et al., 2010b).

4.15 Metabolism pathway analysis

R package ‘scMetabolism’ was used to quantify the metabolism activity at the scRNA-seq dataset. 78 metabolism pathways in KEGG were included in the package. The pathways were further used to evaluate the metabolism activity at the single-cell resolution(Wu et al., 2022).

4.16 Pseudotime trajectory analysis

We applied the single-cell trajectories analysis utilizing Monocle2 using the DDR-Tree and default parameter. Before Monocle analysis, we selected marker genes from the Seurat clustering result and raw expression counts of the cell passed filtering. Based on the pseudotime analysis, branch expression analysis modeling (BEAM Analysis) was applied for branch fate determined gene analysis(Qiu et al., 2017).

4.17 Cell-cell communication analysis

The cell-cell communication was measured by quantification of ligand-receptor pairs among different cell types. Gene expression matrices and metadata with major cell annotations were used as input for the CellChat package (1.6.1)(Jin et al., 2021).

4.18 Spatial transcriptomics data analysis.

Spatial Transcriptomics (ST) slides were printed with two identical capture areas from 1 healthy sample and 1 periodontitis sample(Caetano et al., 2023). The capture of gene expression information for ST slides was performed by the Visium Spatial platform of 10x Genomics through the use of spatially barcoded mRNA-binding oligonucleotides in the default protocol. Raw UMI counts spot matrices, imaging data, spot-image coordinates, and scale factors were imported into R using the Seurat package (versions 4.2.2). Normalization across spots was performed with the LogVMR function. Dimensionality reduction and clustering were performed with independent

component analysis (PCA) at resolution 1with the first 30 PCs. Signature scoring derived from scRNA-seq or ST signatures was performed with the ‘AddModuleScore’ function with default parameters in Seurat. Spatial feature expression plots were generated with the SpatialFeaturePlot function in Seurat (versions 3.2.1). To further increase data resolution at a subspot level, we applied the BayesSpace package(Zhao et al., 2021).

4.19 Statistical analysis

GraphPad Prism software (version 6.0, USA) was used for statistical analyses. Data were presented as the mean and standard deviation (SD) in all graphs. Data were analyzed using the unpaired Student’s t-test in order to compare group pairs or ANOVA for multiple group comparisons. Statistical significance was set at $P < 0.05$.

Acknowledgements

This work was supported by the National Natural Science Foundation of China [grant number 82071095, 32370816]. Thanks to all clinical participants for their contribution.

Competing interests

The authors declare that no competing interests exist.

Funding

u National Natural Science Foundation of China, 82071095 and 32370816 for Haibin Xia. The funders had no role in study design, data collection, and interpretation, or the decision to submit the work for publication.

Author contributions

Liangliang Fu: Conceptualization, Investigation, Formal analysis, Supervision, Project administration, Methodology, Writing – original draft; **Chenghu Yin**: Conceptualization, Investigation, Formal analysis, Software, Methodology, Validation, Writing – original draft; **Qin Zhao:** Methodology, Resources, Supervision; **Shuling Guo:** Software, Visualization; **Wenjun Shao:** Data curation, Software; **Ting Xia:** Methodology, Software; **Quan Sun:** Methodology, Visualization; **Liangwen Chen:** Resources, Visualization;**Min Wang:** Funding acquisition, Project administration, Writing – review and editing;**Haibin Xia**: Conceptualization, Funding acquisition, Project administration, Writing – review and editing.

Ethics

Human subjects: All individuals provided written informed consent and this study was supported by the Ethics Committee of School & Hospital China Hospital of Stomatology Wuhan University [WDKQ2024].

The animal tests in this study adhere to the guidelines established by the Animal Research Ethics Committee at the School & Hospital of Stomatology, Wuhan University, China. The Ethics Committee approved the Animal Use research with protocol number 30/2020.

Data availability

Upon a reasonable request, the corresponding author is able to furnish all the essential data that backs up the discoveries of this research. Single-cell RNA-sequencing data obtained in this study are provided in NIH Gene Expression Omnibus (GSE164241, GSE152042 and GSE242714):

References

Alayash Z, Baumeister S-E, Holtfreter B, Kocher T, Baurecht H, Ehmke B, Nolde M, Reckelkamm SL. 2023. Complement C3 as a potential drug target in periodontitis: Evidence from the cis-Mendelian randomization approach. *J Clin Periodontol*. doi:10.1111/jcpe.13894

An JY, Kerns KA, Ouellette A, Robinson L, Morris HD, Kaczorowski C, Park S-I, Mekvanich T, Kang A, McLean JS, Cox TC, Kaeberlein M. 2020. Rapamycin rejuvenates oral health in aging mice. *Elife* **9**:e54318. doi:10.7554/eLife.54318

Aquino-Martinez R, Eckhardt BA, Rowsey JL, Fraser DG, Khosla S, Farr JN, Monroe DG. 2021. Senescent cells exacerbate chronic inflammation and contribute to periodontal disease progression in old mice. *J Periodontol* **92**:1483–1495. doi:10.1002/JPER.20-0529

Aquino-Martinez R, Rowsey JL, Fraser DG, Eckhardt BA, Khosla S, Farr JN, Monroe DG. 2020a. LPS-induced premature osteocyte senescence: Implications in inflammatory alveolar bone loss and periodontal disease pathogenesis. *Bone* **132**:115220. doi:10.1016/j.bone.2019.115220

Aquino-Martinez R, Rowsey JL, Fraser DG, Eckhardt BA, Khosla S, Farr JN, Monroe DG. 2020b. LPS-Induced Premature Osteocyte Senescence: Implications in Inflammatory Alveolar Bone Loss and Periodontal Disease Pathogenesis. *Bone* **132**:115220. doi:10.1016/j.bone.2019.115220

Caetano AJ, Redhead Y, Karim F, Dhami P, Kannambath S, Nuamah R, Volponi AA, Nibali L, Booth V, D'Agostino EM, Sharpe PT. 2023. Spatially resolved transcriptomics reveals pro-inflammatory fibroblast involved in lymphocyte recruitment through CXCL8 and CXCL10. *eLife*. doi:10.7554/eLife.81525

Caetano AJ, Yianni V, Volponi A, Booth V, D'Agostino EM, Sharpe P. 2021. Defining human mesenchymal and epithelial heterogeneity in response to oral inflammatory disease. *Elife* **10**:e62810. doi:10.7554/eLife.62810

Campisi J. 2013. Aging, cellular senescence, and cancer. *Annu Rev Physiol* **75**:685–705. doi:10.1146/annurev-physiol-030212-183653

Chapple ILC, Matthews JB. 2007. The role of reactive oxygen and antioxidant species in periodontal tissue destruction. *Periodontol 2000* **43**:160–232. doi:10.1111/j.1600-0757.2006.00178.x

Coppé J-P, Desprez P-Y, Krtolica A, Campisi J. 2010a. The senescence-associated secretory phenotype: the dark side of tumor suppression. *Annu Rev Pathol* **5**:99–118. doi:10.1146/annurev-pathol-121808-102144

Coppé J-P, Desprez P-Y, Krtolica A, Campisi J. 2010b. The Senescence-Associated Secretory Phenotype: The Dark Side of Tumor Suppression. *Annu Rev Pathol* **5**:99–118. doi:10.1146/annurev-pathol-121808-102144

Ding H, Dai Y, Lei Y, Wang Z, Liu D, Li R, Shen L, Gu N, Zheng M, Zhu X, Zhao G, Hu Y. 2019. Upregulation of CD81 in trophoblasts induces an imbalance of Treg/Th17 cells by promoting IL-6 expression in preeclampsia. *Cell Mol Immunol* **16**:302–312. doi:10.1038/s41423-018-0186-9

Eke PI, Borgnakke WS, Genco RJ. 2020. Recent epidemiologic trends in periodontitis in the USA. *Periodontol 2000* **82**:257–267. doi:10.1111/prd.12323

El-Awady AR, Elashiry M, Morandini AC, Meghil M, Cutler CW. 2022. Dendritic cells a Critical Link to Alveolar Bone loss and Systemic Disease Risk in Periodontitis: Immunotherapeutic Implications. *Periodontol 2000* **89**:41–50. doi:10.1111/prd.12428

González-Osuna L, Sierra-Cristancho A, Cafferata EA, Melgar-Rodríguez S, Rojas C, Carvajal P,

Cortez C, Vernal R. 2022. Senescent CD4+CD28- T Lymphocytes as a Potential Driver of Th17/Treg Imbalance and Alveolar Bone Resorption during Periodontitis. *Int J Mol Sci* **23**:2543. doi:10.3390/ijms23052543

Ha DY, Jung J-S, Choi GH, Ji S. 2022. Polarization of human gingival fibroblasts by Th1-, Th2-, Th17-, and Treg-derived cytokines. *J Periodontal Res* **57**:487–501. doi:10.1111/jre.12978

Huttner EA, Machado DC, de Oliveira RB, Antunes AGF, Hebling E. 2009. Effects of human aging on periodontal tissues. *Spec Care Dentist* **29**:149–155. doi:10.1111/j.1754-4505.2009.00082.x

Jin S, Guerrero-Juarez CF, Zhang L, Chang I, Ramos R, Kuan C-H, Myung P, Plikus MV, Nie Q. 2021. Inference and analysis of cell-cell communication using CellChat. *Nat Commun* **12**:1088. doi:10.1038/s41467-021-21246-9

Jin Y, Takeda Y, Kondo Y, Tripathi LP, Kang S, Takeshita H, Kuhara H, Maeda Y, Higashiguchi M, Miyake K, Morimura O, Koba T, Hayama Y, Koyama S, Nakanishi K, Iwasaki T, Tetsumoto S, Tsujino K, Kuroyama M, Iwahori K, Hirata H, Takimoto T, Suzuki M, Nagatomo I, Sugimoto K, Fujii Y, Kida H, Mizuguchi K, Ito M, Kijima T, Rakugi H, Mekada E, Tachibana I, Kumanogoh A. 2018. Double deletion of tetraspanins CD9 and CD81 in mice leads to a syndrome resembling accelerated aging. *Sci Rep* **8**:5145. doi:10.1038/s41598-018-23338-x

Karam J, Méresse S, Kremer L, Daher W. 2020. The roles of tetraspanins in bacterial infections. *Cell Microbiol* **22**:e13260. doi:10.1111/cmi.13260

Kuang Y, Hu B, Feng G, Xiang M, Deng Y, Tan M, Li J, Song J. 2020. Metformin prevents against oxidative stress-induced senescence in human periodontal ligament cells. *Biogerontology* **21**:13–27. doi:10.1007/s10522-019-09838-x

Lagnado A, Leslie J, Ruchaud-Sparagano M-H, Victorelli S, Hirsova P, Ogrodnik M, Collins AL, Vizioli MG, Habiballa L, Saretzki G, Evans SA, Salmonowicz H, Hruby A, Geh D, Pavelko KD, Dolan D, Reeves HL, Grellscheid S, Wilson CH, Pandanaboyana S, Doolittle M, von Zglinicki T, Oakley F, Gallage S, Wilson CL, Birch J, Carroll B, Chapman J, Heikenwalder M, Neretti N, Khosla S, Masuda CA, Tchkonia T, Kirkland JL, Jurk D, Mann DA, Passos JF. 2021. Neutrophils induce paracrine telomere dysfunction and senescence in ROS-dependent manner. *EMBO J* **40**:e106048. doi:10.15252/embj.2020106048

Neves VCM, Satie Okajima L, Elbahtety E, Joseph S, Daly J, Menon A, Fan D, Volkyte A, Mainas G, Fung K, Dhami P, Pelegrine AA, Sharpe P, Nibali L, Ide M. 2023. Repurposing Metformin for periodontal disease management as a form of oral-systemic preventive medicine. *Journal of Translational Medicine* **21**:655. doi:10.1186/s12967-023-04456-1

New C, Lee Z-Y, Tan KS, Wong AH-P, Wang DY, Tran T. 2021. Tetraspanins: Host Factors in Viral Infections. *Int J Mol Sci* **22**:11609. doi:10.3390/ijms222111609

Oguri Y, Shinoda K, Kim H, Alba DL, Bolus WR, Wang Q, Brown Z, Pradhan RN, Tajima K, Yoneshiro T, Ikeda K, Chen Y, Cheang RT, Tsujino K, Kim CR, Greiner VJ, Datta R, Yang CD, Atabai K, McManus MT, Koliwad SK, Spiegelman BM, Kajimura S. 2020. CD81 Controls Beige Fat Progenitor Cell Growth and Energy Balance via FAK Signaling. *Cell* **182**:563-577.e20. doi:10.1016/j.cell.2020.06.021

Ohtani N, Hara E. 2013. Roles and mechanisms of cellular senescence in regulation of tissue homeostasis. *Cancer Sci* **104**:525–530. doi:10.1111/cas.12118

Qiu X, Mao Q, Tang Y, Wang L, Chawla R, Pliner HA, Trapnell C. 2017. Reversed graph embedding resolves complex single-cell trajectories. *Nat Methods* **14**:979–982.

doi:10.1038/nmeth.4402

Rodier F, Coppé J-P, Patil CK, Hoeijmakers WAM, Muñoz DP, Raza SR, Freund A, Campeau E, Davalos AR, Campisi J. 2009. Persistent DNA damage signalling triggers senescence-associated inflammatory cytokine secretion. *Nat Cell Biol* **11**:973–979. doi:10.1038/ncb1909

Sanz M, Del Castillo AM, Jepsen S, Gonzalez-Juanatey JR, D'Aiuto F, Bouchard P, Chapple I, Dietrich T, Gotsman I, Graziani F, Herrera D, Loos B, Madianos P, Michel JB, Perel P, Pieske B, Shapira L, Shechter M, Tonetti M, Vlachopoulos C, Wimmer G. 2020. Periodontitis and Cardiovascular Diseases. Consensus Report. *Glob Heart* **15**:1. doi:10.5334/gh.400

Saul D, Kosinsky RL, Atkinson EJ, Doolittle ML, Zhang X, LeBrasseur NK, Pignolo RJ, Robbins PD, Niedernhofer LJ, Ikeno Y, Jurk D, Passos JF, Hickson LJ, Xue A, Monroe DG, Tchkonia T, Kirkland JL, Farr JN, Khosla S. 2022. A new gene set identifies senescent cells and predicts senescence-associated pathways across tissues. *Nat Commun* **13**:4827. doi:10.1038/s41467-022-32552-1

Uriarte SM, Hajishengallis G. 2023. Neutrophils in the periodontium: Interactions with pathogens and roles in tissue homeostasis and inflammation. *Immunol Rev* **314**:93–110. doi:10.1111/imr.13152

Wielento A, Lagosz-Cwik KB, Potempa J, Grabiec AM. 2023. The Role of Gingival Fibroblasts in the Pathogenesis of Periodontitis. J Dent Res 102:489–496. doi:10.1177/00220345231151921

Williams DW, Greenwell-Wild T, Brenchley L, Dutzan N, Overmiller A, Sawaya AP, Webb S, Martin D, NIDCD/NIDCR Genomics and Computational Biology Core, Hajishengallis G, Divaris K, Morasso M, Haniffa M, Moutsopoulos NM. 2021. Human oral mucosa cell atlas reveals a stromal-neutrophil axis regulating tissue immunity. *Cell* 184:4090-4104.e15. doi:10.1016/j.cell.2021.05.013

Wolff L, Dahlén G, Aeppli D. 1994. Bacteria as Risk Markers for Periodontitis. *J Periodontol* **65 Suppl 5S**:498–510. doi:10.1902/jop.1994.65.5s.498

Wu Y, Yang S, Ma J, Chen Z, Song G, Rao D, Cheng Y, Huang S, Liu Y, Jiang S, Liu J, Huang X, Wang X, Qiu S, Xu J, Xi R, Bai F, Zhou J, Fan J, Zhang X, Gao Q. 2022. Spatiotemporal Immune Landscape of Colorectal Cancer Liver Metastasis at Single-Cell Level. *Cancer Discov* **12**:134–153. doi:10.1158/2159-8290.CD-21-0316

Yipp BG, Petri B, Salina D, Jenne CN, Scott BNV, Zbytnuik LD, Pittman K, Asaduzzaman M, Wu K, Meijndert HC, Malawista SE, de Boisfleury Chevance A, Zhang K, Conly J, Kubes P. 2012. Dynamic NETosis is Carried Out by Live Neutrophils in Human and Mouse Bacterial Abscesses and During Severe Gram-Positive Infection. *Nat Med* **18**:1386–1393. doi:10.1038/nm.2847

Zhang Z, Cui F, Lin C, Zhao L, Wang C, Zou Q. 2021. Critical downstream analysis steps for single-cell RNA sequencing data. *Brief Bioinform* **22**:bbab105. doi:10.1093/bib/bbab105

Zhao E, Stone MR, Ren X, Guenthoer J, Smythe KS, Pulliam T, Williams SR, Uytingco CR, Taylor SEB, Nghiem P, Bielas JH, Gottardo R. 2021. Spatial transcriptomics at subspot resolution with BayesSpace. *Nat Biotechnol* **39**:1375–1384. doi:10.1038/s41587-021-00935-2

Figures

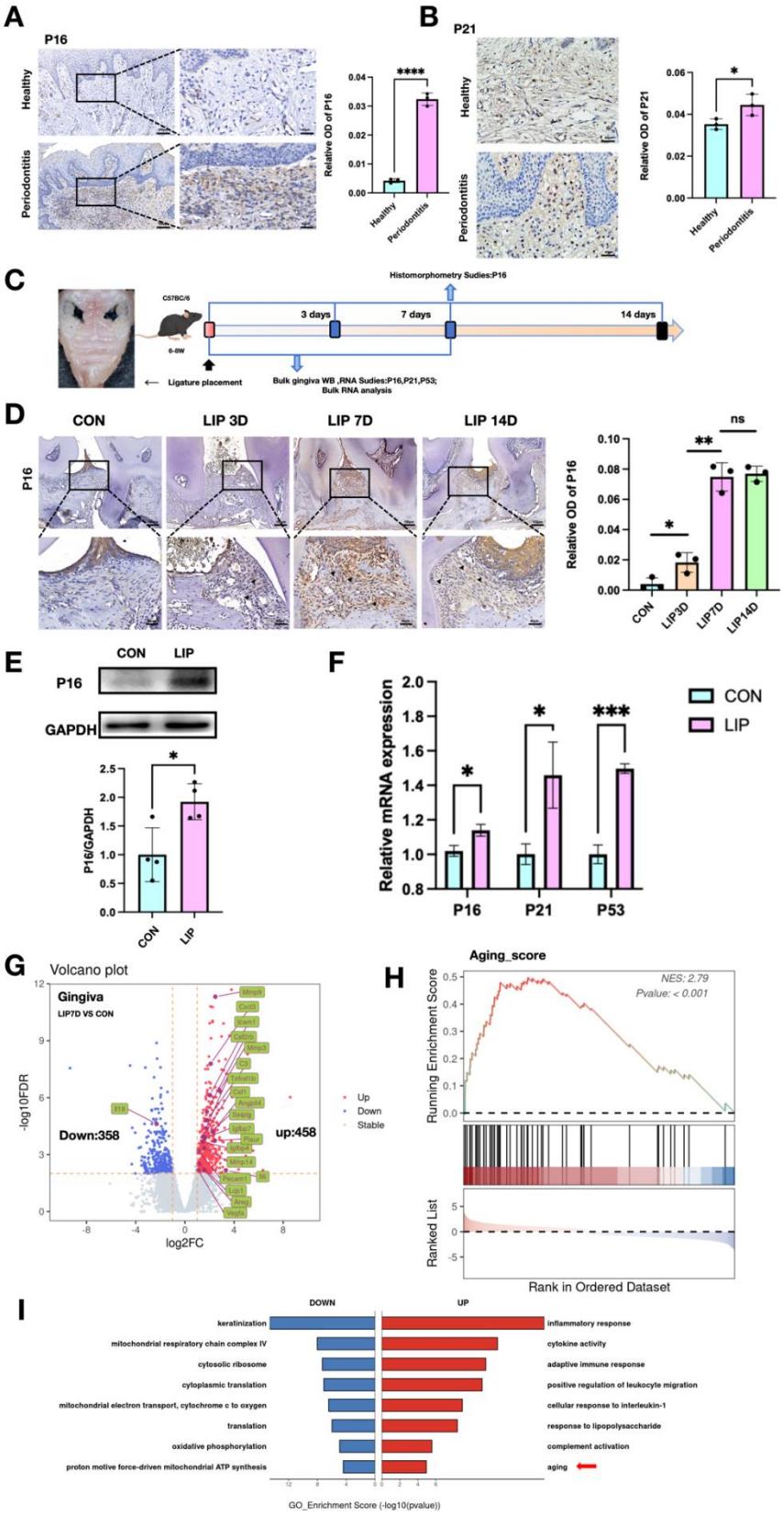
A
P16
Healthy
Periodontitis
Relative OD of P16
Healthy
Periodontitis
B
P21
Healthy
Periodontitis
Relative OD of P21
Healthy
Periodontitis
C
C57BC/6
6-8W
Ligature placement
Histomorphometry Sudies:P16
3 days
7 days
14 days
Bulk gingiva WB ,RNA Sudies:P16,P21,P53;
Bulk RNA analysis
D
CON
LIP 3D
LIP 7D
LIP 14D
P16
Relative OD of P16
ns
CON
LIP3D
LIP7D
LIP14D
E
CON
LIP
P16
GAPDH
P16/GAPDH
CON
LIP
F
Relative mRNA expression
CON
LIP
P16
P21
P53
G
Volcano plot
Gingiva
LIP7D VS CON
Down:358
up:458
-log10FDR
log2FC
Up
Down
Stable
H
Aging_score
NES: 2.79
Pvalue: < 0.001
Running Enrichment Score
Ranked List
Rank in Ordered Dataset
I
DOWN
UP
keratinization
mitochondrial respiratory chain complex IV
cytosolic ribosome
cytoplasmic translation
mitochondrial electron transport, cytochrome c to oxygen
translation
oxidative phosphorylation
proton motive force-driven mitochondrial ATP synthesis
inflammatory response
cytokine activity
adaptive immune response
positive regulation of leukocyte migration
cellular response to interleukin-1
response to lipopolysaccharide
complement activation
aging
GO_Enrichment Score (-log10(pvalue))

Figure 1. Accelerated cellular senescence along with periodontitis progression. (**A and B**) IHC staining and semi-quantification of P16 and P21 in healthy and periodontitis patient gingiva (n=3). (**C**) Strategy of ligature-induced periodontitis (LIP) mouse model. (**D**) IHC staining and semi-quantification of P16 in mouse gingiva of health and LIP post 3D, 7D and 14D (n=3). (**E**) Western blot images and semi-quantification of P16 protein levels in control and LIP post 7D mouse gingiva (n=3). (**F**) qPCR analysis of P16, P21and P53 in control and LIP post 7D mouse gingiva (n=3). (**G**) Volcano plots displaying the differentially expressed genes in mouse gingiva among LIP 7D compared to the control. Representative aging related genes are indicated as green. blue dots indicate differentially down-regulated genes; red dots indicate differentially up-regulated genes. Significantly different expression gene with log2FC > 1 and FDR < 0.05. (**H**) GSEA enrichment analysis of aging gene sets in differentially expressed genes in mouse gingiva. (**I**) GO enrichment analysis with genes upregulated (red) and downregulated (blue) genes shown in (G). Data are mean ± SD. *p<0.05, **p<0.01, ***p<0.001. ****p<0.0001.

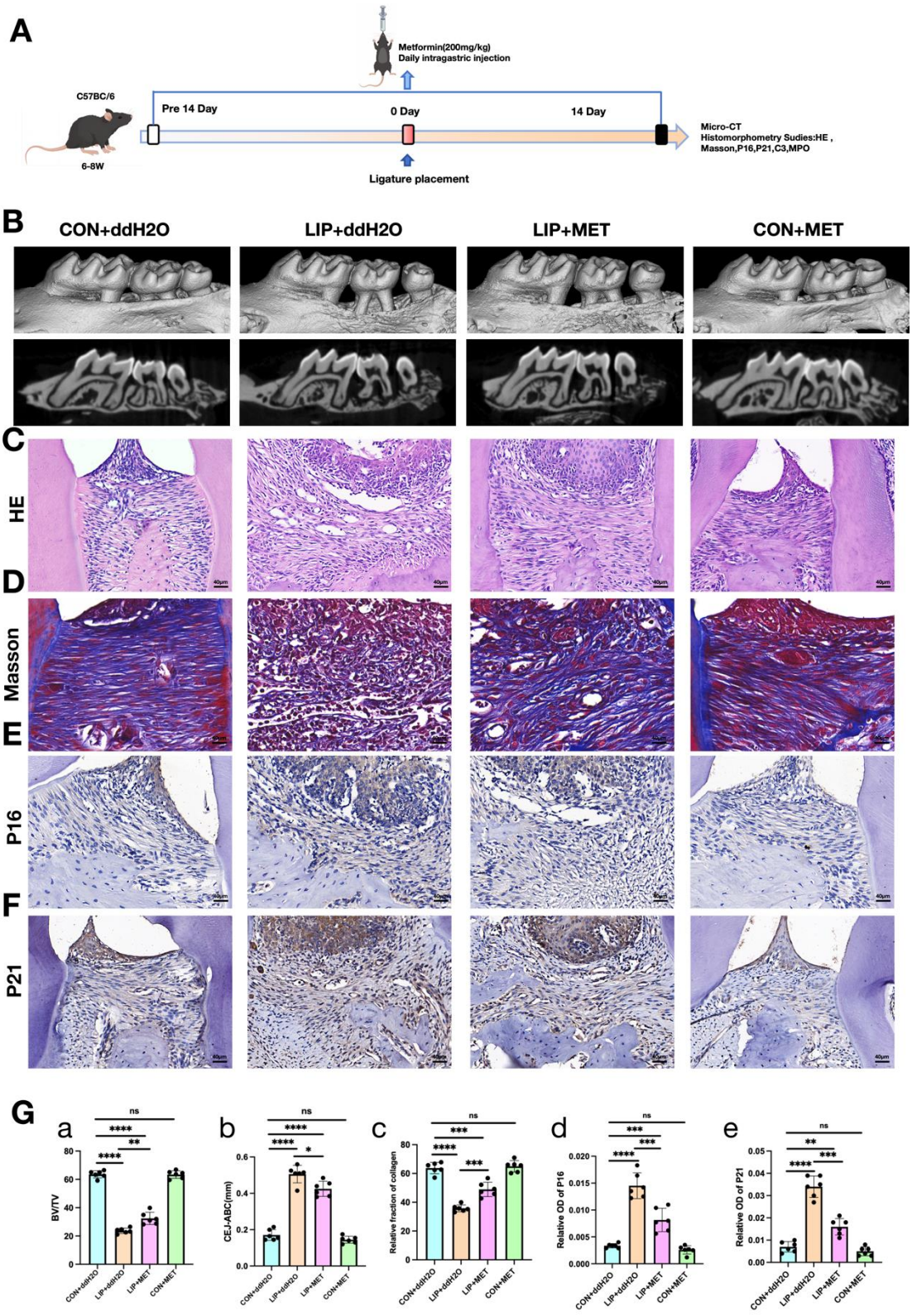

Figure 2. Inhibition of cellular senescence alleviates bone damage in ligation induced periodontitis (LIP) murine models. (**A**) Establishment of a mouse model of periodontitis treated with metformin. (**B**) Micro-CT images and 3-D visualization of the maxilla. and quantified by the BV/TV ratio (**Ga**) the CEJ-ABC distance (**Gb**) (**C**) Representative images of HE staining. (**D**)

Representative images of Masson staining and quantification of collagen fiber(Gc), in which collagen fibers were stained into blue（**E and F**）IHC staining and semi-quantification (Gd) of P16. （**F**）IHC staining and semi-quantification (**Ge**) of P21. N = 6, *P <= 0.05, **P<= 0.01, ***P<= 0.001, ****P<= 0.0001.

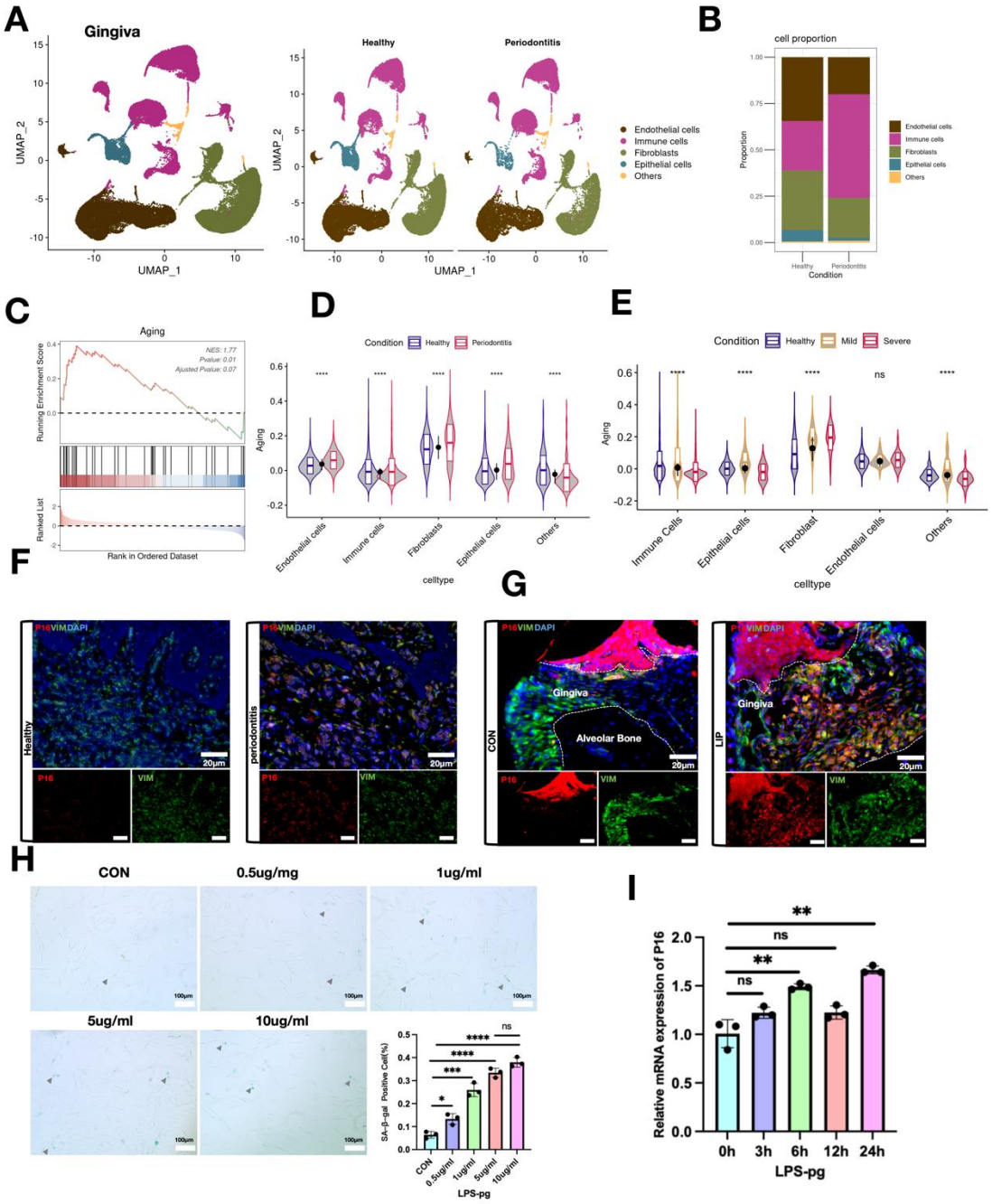

Figure 3. Gingival fibroblasts are the main senescent cell type in periodontitis. (**A**) UMAP diagram and single-cell annotation of cells clusters for the healthy and periodontitis samples from GSE164241. (**B**) Histogram of gingival tissue cell ratio in healthy and periodontitis patients. (**C**) GSEA enrichment analysis of aging pathway in differentially expressed genes in fibroblasts among periodontitis and healthy gingiva. (**D**) The violin plot showing aging score of subgroups in healthy and periodontitis gingiva. (**E**) The violin plot showing aging score in subgroups in gingiva of healthy, mild and severe periodontitis patient from GSE152042. (**F and G**) IF staining of P16 (red), VIM (green), and nuclei (blue) in healthy and periodontitis patient

gingiva or in control and LIP mouse gingiva. (**H**) β-Galactosidase staining and semi-quantification of HGF stimulated by different concentrations of pg-LPS. White arrow indicates positive cells. (**I**) qPCR analysis of P16 expression of HGF stimulated by different concentrations of pg-LPS. *P <= 0.05, **P<= 0.01, ***P<= 0.001, ****P<= 0.0001.

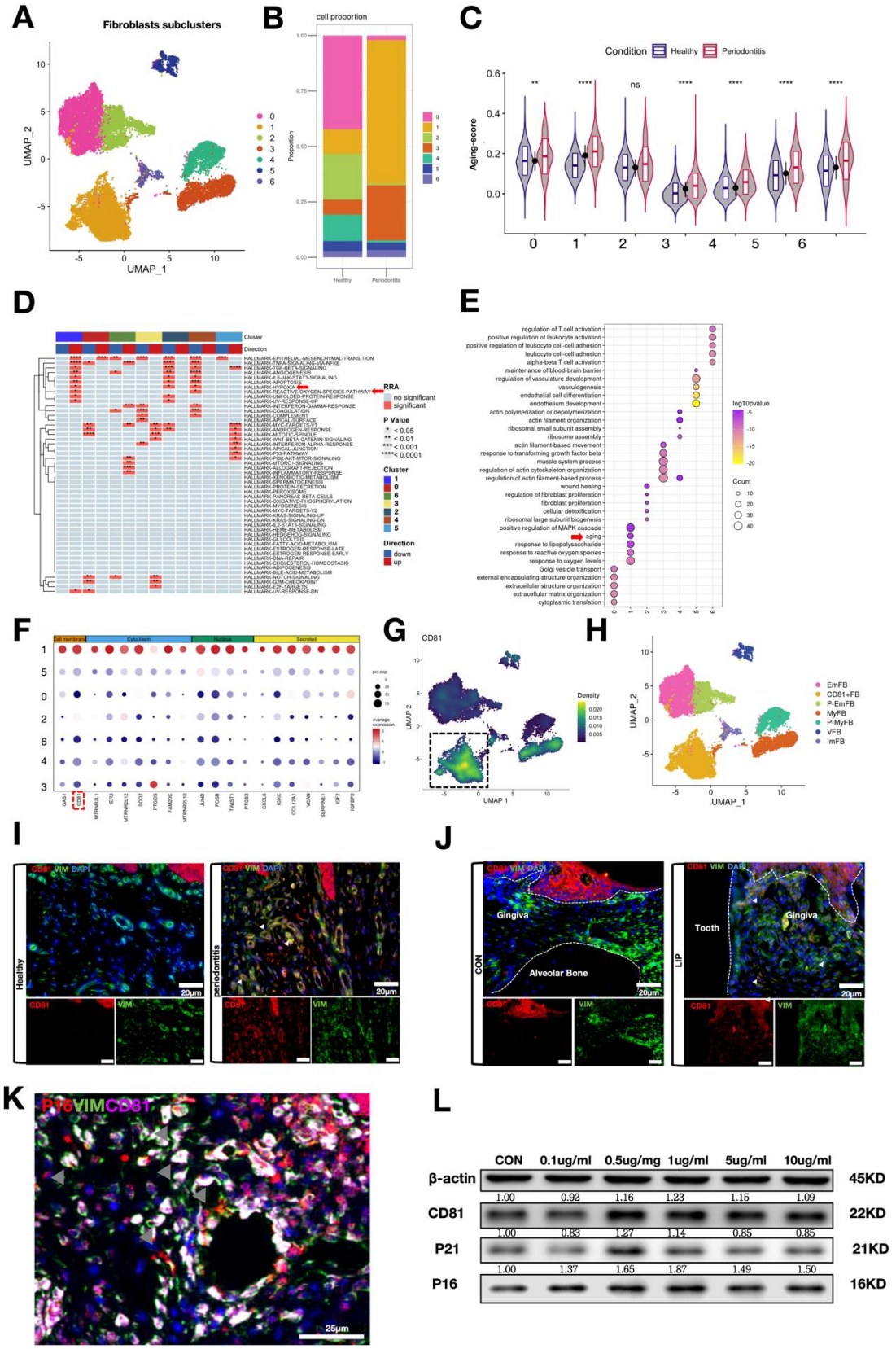

Figure 4. CD81 is identified as the representative marker of senescent gingival fibroblast. (**A**) UMAP diagram illustrated the cell clusters of fibroblasts. (**B**) Histogram of fibroblasts subclusters

ratio in healthy and periodontitis gingiva. (**C**) The violin plot showing aging score of fibroblasts subclusters in healthy and periodontitis gingiva. (**D**) Enrichment analysis on Hallmark Gene-sets from GSEA. (**E**) GO enrichment analysis of fibroblasts subclusters. (**F**) Localization of the top 20 marker gene in fibroblasts subcluster 1. (**G**) Density map of CD81 expression. (**H**) Single-cell annotation of fibroblasts subclusters. (**I, J**) IF staining of CD81 (red), VIM (green) and nuclei (blue) in healthy and periodontitis patient gingiva or in healthy and LIP mouse gingiva. White arrow indicates double positive cells. (**K**) IF staining of P16 (red), VIM (green), CD81 (purple), and nuclei (blue) in LIP mouse gingiva. gray arrow indicates triple positive cells. (**L**) Western blot image and semi-quantification of human P16, P21 and CD81 protein levels of HGF stimulated by different concentrations of pg-LPS. * P <= 0.05, **P<= 0.01, ***P<= 0.001, ****P<= 0.0001.

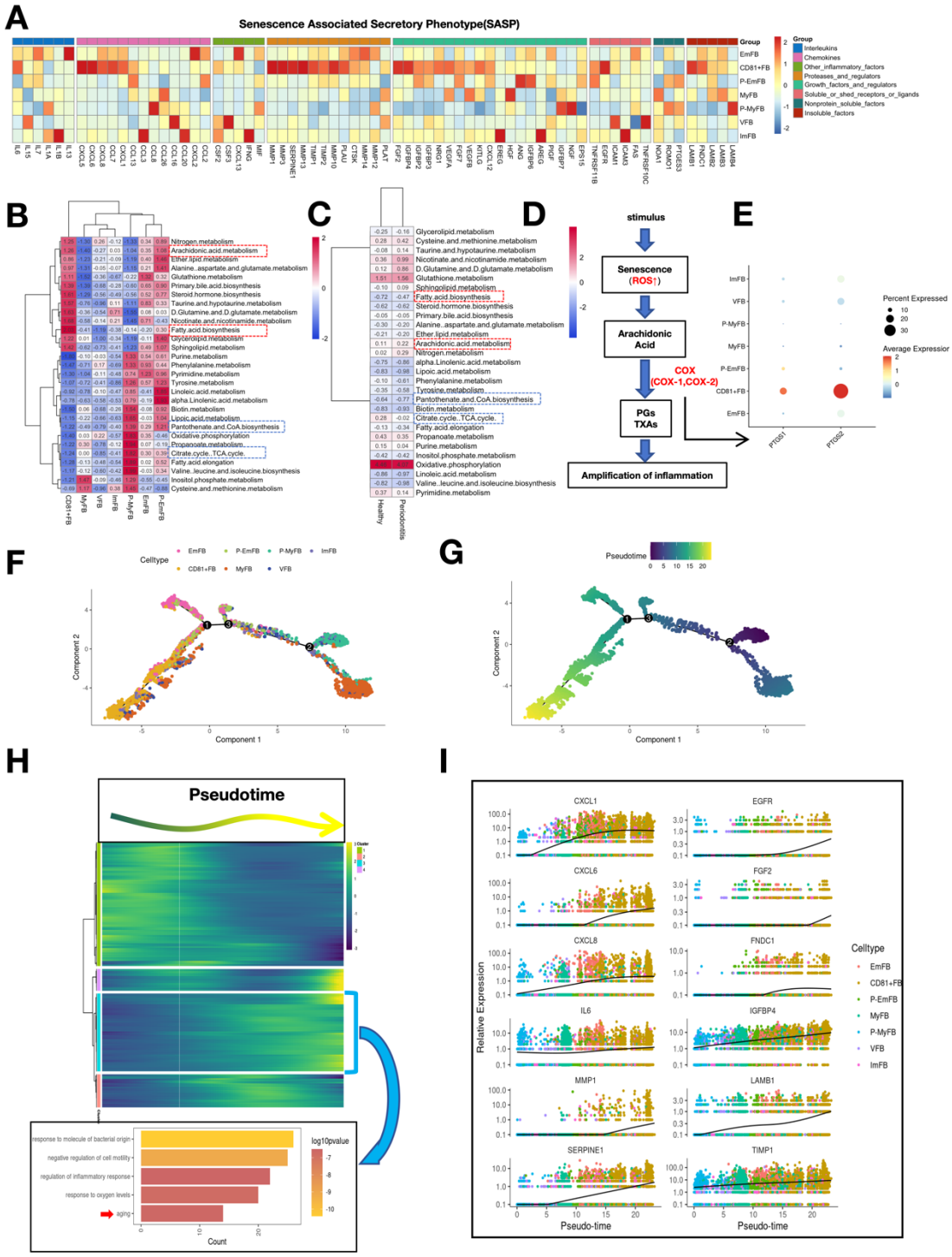

Figure 5. CD81$^+$ gingival fibroblasts are terminally differentiational cell with high SASP expression and metabolism alteration. (**A**) Heatmap showing the relative expression for SASP genes in each fibroblast subclusters. (**B**) The heatmap representing metabolic pathways in each fibroblast subclusters. (**C**) The heatmap representing metabolic pathways between healthy and periodontitis gingiva. (**D**) The flow chart representing the metabolism of arachidonic acid. (**E**) The dot plot representing that COX1 and COX2 are significantly increased in CD81$^+$ gingival fibroblasts. (**F**) Trajectory reconstruction of all gingival fibroblast clusters (**G**) Monocle

pseudotime analysis revealing the progression of gingival fibroblast clusters. (**H**) Upper panel: Heatmap showing the scaled expression of differently expressed genes in trajectory as in (G), cataloged into four gene clusters (labels on left). Bottom panel: GO analysis of expressed genes whose expression increases as the differentiation trajectory progresses. (**I**) SASP-related genes with increased expression as the differentiation trajectory progresses. * P <= 0.05, **P<= 0.01, ***P<= 0.001, ****P<= 0.0001.

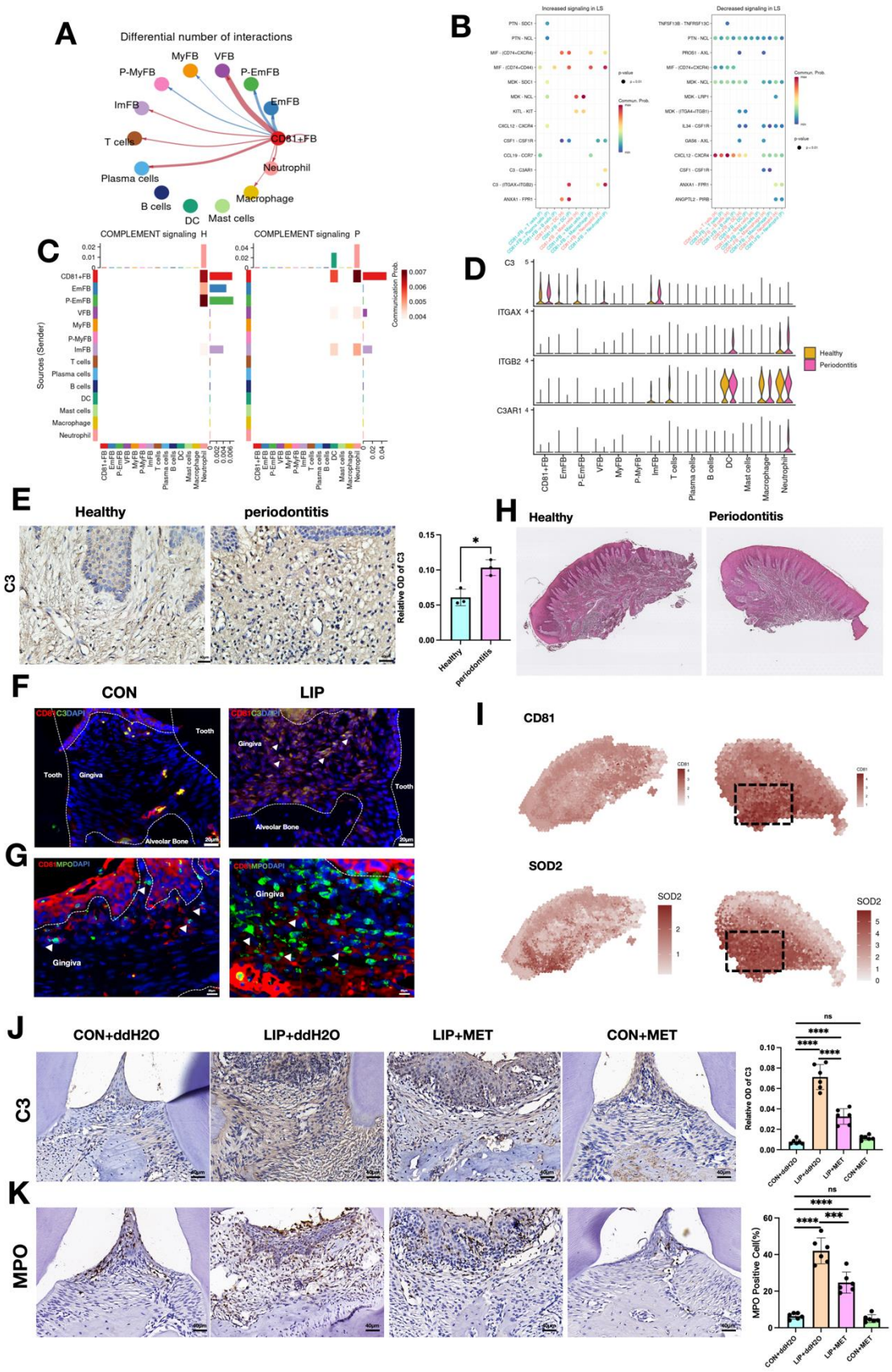

Figure 6. CD81^{+}fibroblasts recruit neutrophils via C3/C3aR1 axis. (**A**) The relative number and intensity of interactions between fibroblasts and neutrophil in periodontitis gingiva.

(**B**)Significant increased (left) and decreased (right) Ligand-Receptor interaction derived from $CD81^+$fibroblasts. (**C**) The heatmap showing the communication patterns of the complement signaling pathway between fibroblasts and immune cell type. (**D**) The expression level of four representative genes in complement signaling pathway. (**E**) IHC staining and semi-quantification of C3 in healthy and periodontitis gingiva. (**F**) IF staining of CD81 (red), C3 (green), and nuclei (blue) in control and LIP mouse gingiva. (**G**) IF staining of CD81 (red), MPO (green), and nuclei (blue) in control and LIP mouse gingiva. (**H**) H&E image of the representative inflamed oral mucosa from GSE152042. (**I**) Representative spatial mapping of CD81 and SOD2 in health and periodontal disease showing co-localization in $CD81^+$ fibroblasts and neutrophil in the periodontal disease. (**J** and **K**) IHC staining and semi-quantification of C3 and MPO in periodontitis treated by metformin. *P <= 0.05, **P<= 0.01, ***P<= 0.001, ****P<= 0.0001.

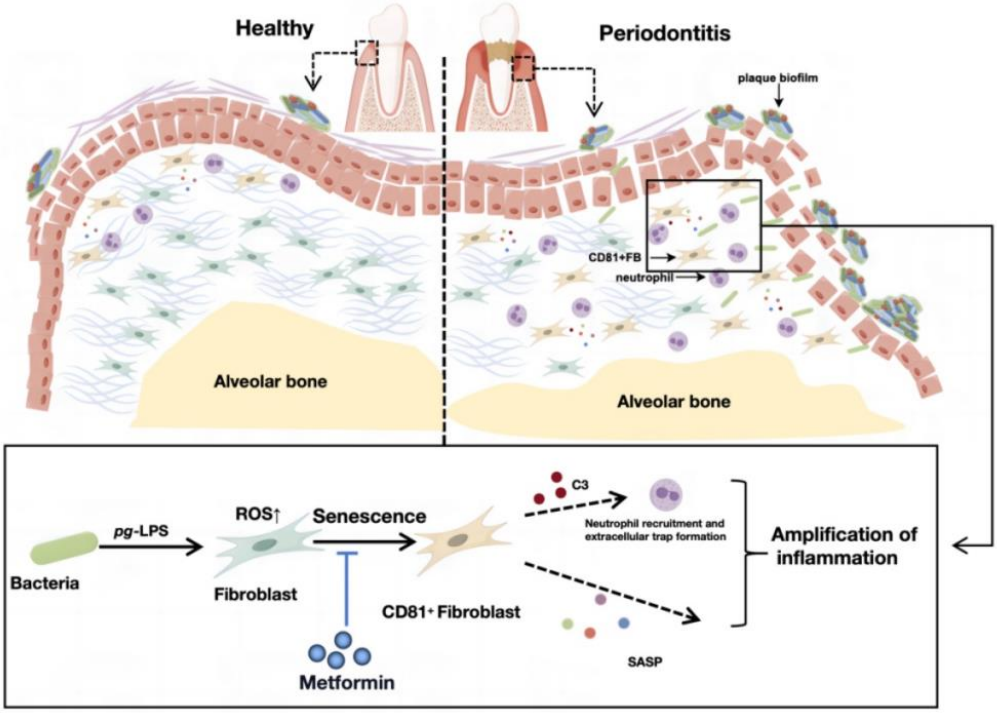

Figure 7. Schematic overview of the CD81^{+} senescent gingival fibroblast-neutrophil axis in periodontitis progression. We propose that the initial periodontal inflammation is triggered by the CD81^{+} senescent gingival fibroblast induced by bacterial virulence like Pg-LPS. CD81+ senescent gingival fibroblast could exaggerate inflammation in the periodontal tissue via secreting SASPs and recruiting neutrophils by C3. In addition, metformin could alleviate the cellular senescence of the fibroblast and rescue the uncontrolled inflammation and bone resorption.